scientific reports

Check for updates

OPEN

Myopia prediction for children and adolescents via time-aware deep learning

Junjia Huang[1], Wei Ma[2]✉, Rong Li[3], Na Zhao[4,5] & Tao Zhou[1,5]✉

This is a retrospective analysis. Quantitative prediction of the children's and adolescents' spherical equivalent based on their variable-length historical vision records. From October 2019 to March 2022, we examined uncorrected visual acuity, sphere, astigmatism, axis, corneal curvature and axial length of 75,172 eyes from 37,586 children and adolescents aged 6–20 years in Chengdu, China. 80% samples consist of the training set, the 10% form the validation set and the remaining 10% form the testing set. Time-Aware Long Short-Term Memory was used to quantitatively predict the children's and adolescents' spherical equivalent within two and a half years. The mean absolute prediction error on the testing set was 0.103 ± 0.140 (D) for spherical equivalent, ranging from 0.040 ± 0.050 (D) to 0.187 ± 0.168 (D) if we consider different lengths of historical records and different prediction durations. Time-Aware Long Short-Term Memory was applied to captured the temporal features in irregularly sampled time series, which is more in line with the characteristics of real data and thus has higher applicability, and helps to identify the progression of myopia earlier. The overall error 0.103 (D) is much smaller than the criterion for clinically acceptable prediction, say 0.75 (D).

Myopia is a global public health concern. It is estimated that 57% of countries will have a myopia prevalence of more than 50% by 2050[1]. The World Health Organization reported in 2019 that at least 2.2 billion people have a vision impairment, of whom at least 1 billion have a vision impairment that could have been prevented[2]. As myopia is currently difficult to be cured completely, it is vital to prevent its onset and progression. An early and appropriate intervention can effectively mitigate the risks and consequences related to myopia[3]. The spherical equivalent (SE) is the basis for screening and diagnosing myopia[4]. Quantitative prediction of SE can indicate the specific changes in the progression of myopia, and help in designing targeted interventions in advance. Previous studies have reported a number of risk factors for the onset or progression of myopia, including age, gender, heredity, outdoor activities, etc.[5–7]. Matsumura et al.[8] suggested that the historical progression of myopia is associated with future changes in visual acuity. Therefore, we believe that the historical vision records, together with other demographic information, can be used to quantitatively predict SE.

In recent years, a growing body of research has considered the prediction of myopia or high myopia in different populations[9]. Most known studies used traditional models like linear regression, support vector machines, decision trees, and so on[10–17]. In comparison, deep learning can be trained with complex and nonlinear parameters to learn data structures[18], and is deemed to perform better than traditional models in a variety of medical prediction tasks[19–22]. However, there are only few applications of deep learning in myopia prediction.

Spadon et al.[23] argued that the temporal dynamics provides valuable information in addition to static symptom observation. However, in usual vision records, the uneven distribution of time intervals between historical records makes the extraction of temporal features very difficult. This paper uses Time-Aware Long Short-Term Memory (T-LSTM) to capture the temporal features in irregularly sampled time series, and to quantitatively predict children's and adolescents' SE based on their variable-length historical vision records. The proposed method is widely applicable.

[1]Big Data Research Center, University of Electronic Science and Technology of China, Chengdu 611731, People's Republic of China. [2]Department of Ophthalmology, West China Hospital, Sichuan University, Chengdu 610041, People's Republic of China. [3]Eye See Inc., Chengdu 610041, People's Republic of China. [4]Key Laboratory in Software Engineering of Yunnan Province, Yunnan University, Kunming 650091, People's Republic of China. [5]Computational Education Lab, SeekingTao Tech. Inc., Chengdu 610095, People's Republic of China. ✉email: mawei@wchscu.cn; zhutou@ustc.edu

Features	Statistics
Id	
Check date	
School age groups	1 (69.3%): elementary school, 2 (23.7%): middle school, 3 (7.0%): high school
Gender	0 (48.5%): female, 1 (51.5%): male
Age (years)	10.38 ± 2.90, [6, 20]
Correction method	0 (65.0%): uncorrected, 1 (35.0%): spectacles glasses
Uncorrected visual acuity	0.31 ± 0.32, [− 0.3, 1]
Sphere (D)	− 1.21 ± 1.75, [− 11.25, 8.75]
Astigmatism (D)	− 0.71 ± 0.65, [− 6.75, 0.00]
Axis (°)	With-the-rule astigmatism (87.5%), against-the-rule astigmatism (4.5%), oblique astigmatism (8.0%), [0, 180]
Corneal curvature K1 (D)	42.54 ± 1.36, [37.05, 48.63]
Corneal curvature K2 (D)	43.87 ± 1.51, [37.58, 50.00]
Axial length (mm)	23.99 ± 1.14, [18.59, 29.86]
Myopia	0 (46.5%): no myopia, 1 (53.5%): myopia
The level of myopia	0 (46.5%): no myopia, 1 (37.8%): low myopia, 2 (14.5%): moderate myopia, 3 (1.2%): high myopia
SE	− 1.57 ± 1.85, [− 12.63, 8.25]

Table 1. Feature description. Discrete variables: value (percentage). Continuous variables: mean ± standard deviation, [min, max]. Axis values follow a bimodal distribution, so the mean value and standard deviation are less meaningful. Therefore, we treat it as a quasi-categorical variable with three classes: with-the-rule astigmatism ($Axis < 30^\circ$ or $Axis > 150^\circ$), against-the-rule astigmatism ($60^\circ \leq Axis \leq 120^\circ$), and oblique astigmatism ($30^\circ \leq Axis < 60^\circ$ or $120^\circ < Axis \leq 150^\circ$). Detailed distribution is shown in Fig. 1.

Methods

Data description. The dataset for this study contains 232,244 historical vision records from 37,586 school-aged children and adolescents (aged 6–20 years) in Chengdu, China. They were collected by Eye See Inc. from October 2019 to March 2022 through unscheduled refractive screening in schools. Eye See Inc. is a company in Chengdu, China, providing medical services for myopia prevention and control. As of December 2022, Eye See Inc. has completed myopia screening for more than 1,600,000 children and adolescents in more than 2000 schools. Tumbling E Logarithmic Visual Acuity Chart (under the National Standard of the People's Republic of China No. GB11533-2011), Slit Lamp Microscope (SL-3G, Topcon), Auto Kerato-Refractometer (KR-800, Topcon), and Optical Biometer (AL-Scan, Nidek) were used for data collection. Inclusion criteria: elementary, middle and high school students between the ages of 6 and 20. Exclusion criteria: students who did not obtain consent from their parents or their guardians, students who were unable to cooperate with the examination or did not complete the examination due to intellectual or physical reasons. The following examinations were performed based on the standard clinical protocols: (1) distant vision examination; (2) slit-lamp microscope examination; (3) pre-cycloplegic objective refractive examination; (4) axial length measurement.

The myopia diagnostic criteria associated were developed in accordance with the Consensus on Myopia Management for Asia 2021, published by the Asia Optometric Management Academy (AOMA) and Asia Optometric Congress (AOC)[4]. Based on SE when the eye is relaxed, the criterion of myopia is $SE \leq -0.5\ (D)$, and the level of myopia is classified as follows: (1) low myopia: $-3.0\ (D) < SE \leq -0.5\ (D)$; (2) moderate myopia: $-6.0\ (D) < SE \leq -3.0\ (D)$; (3) high myopia: $SE \leq -6.0\ (D)$.

The cleaned dataset contains 75,172 eyes (samples) of 37,586 children and adolescents. Each sample is associated with 2–6 records. The number of samples with 2, 3, 4, 5 and 6 records is 27,015, 18,732, 25,109, 4,314 and 2, respectively. The interval time between the first record and the last record for any sample ranges from 1 (< 1 *quarter*) to 10 (≥ 9 *quarters*, < 10 *quarters*). Each record is associated with 16 features, as described in Table 1. Figure 1 shows distributions of these features. A possible time-series data for an adolescent is shown in Table 2.

Data preprocessing. Firstly, in order to exclude the interference between categories of the original sequential encoding, one-hot encoding was performed for the unordered categorical features, say correction method and gender. It creates unit vectors for each option within the categorical feature, where the dimensionality of the vector equals the number of categories[24]. For example, a possible one-hot encoding for gender, as above, is male: (1, 0), and female: (0, 1).

After one-hot encoding, the features were standardized except for Id and Check date to speed up the convergence of the model. The standardization rescales the sample mean to zero ($\mu = 0$) and variance to unit ($\sigma = 1$)[25], as

$$x' = \frac{x - \mu}{\sigma}. \tag{1}$$

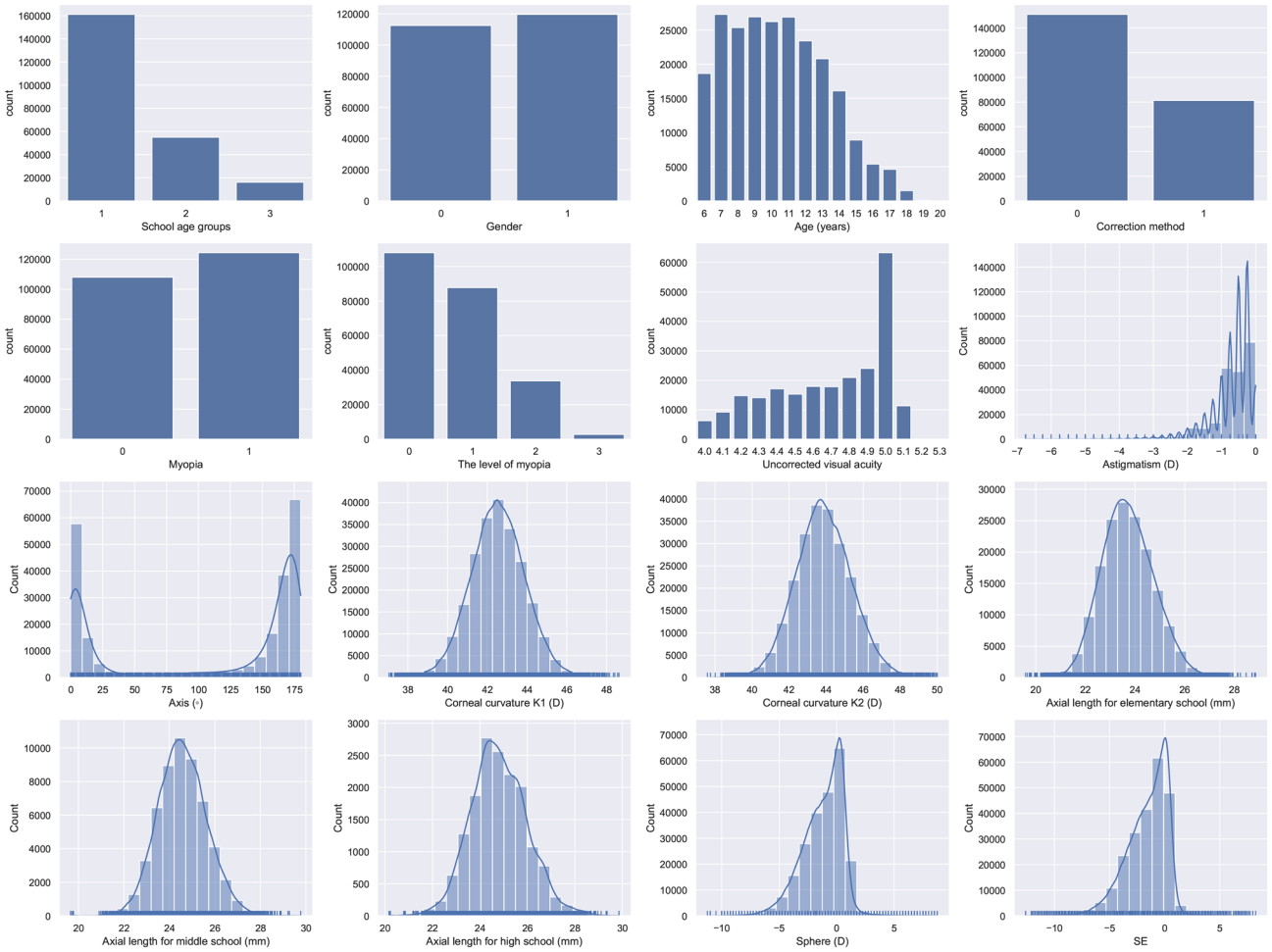

Figure 1. The distributions of features. Particularly, as children and adolescents grow taller over time, the size of eyeballs will gradually elongate, so the overall distribution of axial lengths is divided to three distributions, each corresponds to one age group.

1	2019-10-21	1	0	11	0	− 0.1	0	− 0.5	159	43.16	45.06	23.16	0	0	− 0.25
1	2020-9-27	2	0	11	0	0.1	− 0.25	− 0.75	165	43.32	45.06	23.38	1	1	− 0.625
1	2021-4-28	2	0	12	0	0.4	− 1.25	− 0.75	164	43.21	45.24	23.74	1	1	− 1.625
1	2021-11-4	2	0	13	0	0.2	− 1.5	− 0.5	162	43.53	45.15	23.91	1	1	− 1.75
1	2022-3-9	2	0	13	0	0.3	− 1.25	− 0.75	170	43.32	45	23.85	1	1	− 1.625

Table 2. The time-series data for an adolescent whose Id is 1. The headers of the table are id, check date, school age groups, gender, age, correction method, uncorrected visual acuity, sphere, astigmatism, axis, corneal curvature K1, corneal curvature K2, axial length, myopia, the level of myopia, SE in that order.

To increase the sample size, the historical records of a child or an adolescent were split into several samples, ensuring that all input data used for training and predicting is recorded before the label (i.e., the SE value). For example, a child's or an adolescent's 4 records (a, b, c, d) can be split into 11 samples as shown in Table 3.

The number of samples in the dataset increased to 490,420 after the data preprocessing. The sample sizes are 277,035, 162,348, 46,709, 4,326 and 2 for sequence lengths of 1, 2, 3, 4 and 5, respectively. Particularly, sample with sequence length 5 is too few to be included in the training. The dataset was then divided into layers by the lengths of sequences. Each layer was further divided into training set (80%), validation set (10%) and testing set (10%).

LSTM. Recurrent Neural Network (RNN) is a neural network structure that can effectively link contextual information to achieve long term memory, but suffer from the problem of gradient vanishing or exploding[26,27]. To solve this challenge, Hochreiter et al.[28] proposed the method named Long Short-Term Memory (LSTM),

Input data	Label	Time interval
[a]	[b]	[ab]
[a]	[c]	[ac]
[a]	[d]	[ad]
[b]	[c]	[bc]
[b]	[d]	[bd]
[c]	[d]	[cd]
[a, b]	[c]	[ab, bc]
[a, b]	[d]	[ab, bd]
[a, c]	[d]	[ac, cd]
[b, c]	[d]	[bc, cd]
[a, b, c]	[d]	[ab, bc, cd]

Table 3. The enhanced samples from a child's or an adolescent's 4 records (a, b, c, d). The time interval [ab] means the interval between record a and record b, in quarter.

which is a variant of RNN, combining short-term memory with long-term memory through gate control. LSTM solves the problem of gradient vanishing to a certain extent and allows for the learning of long-term dependent information.

Standard LSTM unit (Fig. 2a) consists of a forget gate, an input gate, an output gate and a cell state. The current state h_t is influenced by the previous state h_{t-1} and the current input x_t.

Forget gate:

$$f_t = \sigma\left(W_f x_t + U_f h_{t-1} + b_f\right) \tag{2}$$

Input gate:

$$i_t = \sigma(W_i x_t + U_i h_{t-1} + b_i) \tag{3}$$

$$\widetilde{C}_t = tanh(W_c x_t + U_c h_{t-1} + b_c) \tag{4}$$

Output gate:

$$o_t = \sigma(W_o x_t + U_o h_{t-1} + b_o) \tag{5}$$

$$h_t = o_t \cdot tanh(C_t) \tag{6}$$

Cell state:

$$C_t = f_t C_{t-1} + i_t \widetilde{C}_t \tag{7}$$

where σ and $tanh$ represent the activation functions, and W, U and b are the learnable parameters.

The standard LSTM assumes that the time intervals between sequential elements are uniformly distributed, and thus cannot handle the problem with irregular time intervals.

T-LSTM. T-LSTM (Fig. 2b) introduces time interval information based on the standard LSTM, and attenuates the short-term memory according to the time intervals in order to capture the temporal dynamics of the sequential data with temporal irregularity[29]. T-LSTM accepts two inputs: the current record and the current time step elapsed. T-LSTM differs from the standard LSTM primarily in the subspace decomposition of the previous time step, which adjusts the short-term memory according to the time intervals between records. The subspace decomposition method does not change the effect of the current input on the current output, but changes the effect of the previous memory on the current output. Specifically, T-LSTM adds the following features to the standard LSTM: (1) Short-term memory C^S_{t-1}, obtained through the memory of the previous time step, as

$$C^S_{t-1} = tanh(W_d C_{t-1} + b_d). \tag{8}$$

(2) Discounted short-term memory $\hat{C}^S_{t-1}$, obtained by weighting C^S_{t-1} with time elapsed, as

$$\hat{C}^S_{t-1} = C^S_{t-1} \cdot g(\Delta_t). \tag{9}$$

(3) Long-term memory C^T_{t-1}, which is the supplementary subspace of short-term memory, as

$$C^T_{t-1} = C_{t-1} - C^S_{t-1}. \tag{10}$$

(4) Adjusted previous memory C^*_{t-1}, obtained through combining discounted short-term memory and long-term memory, as

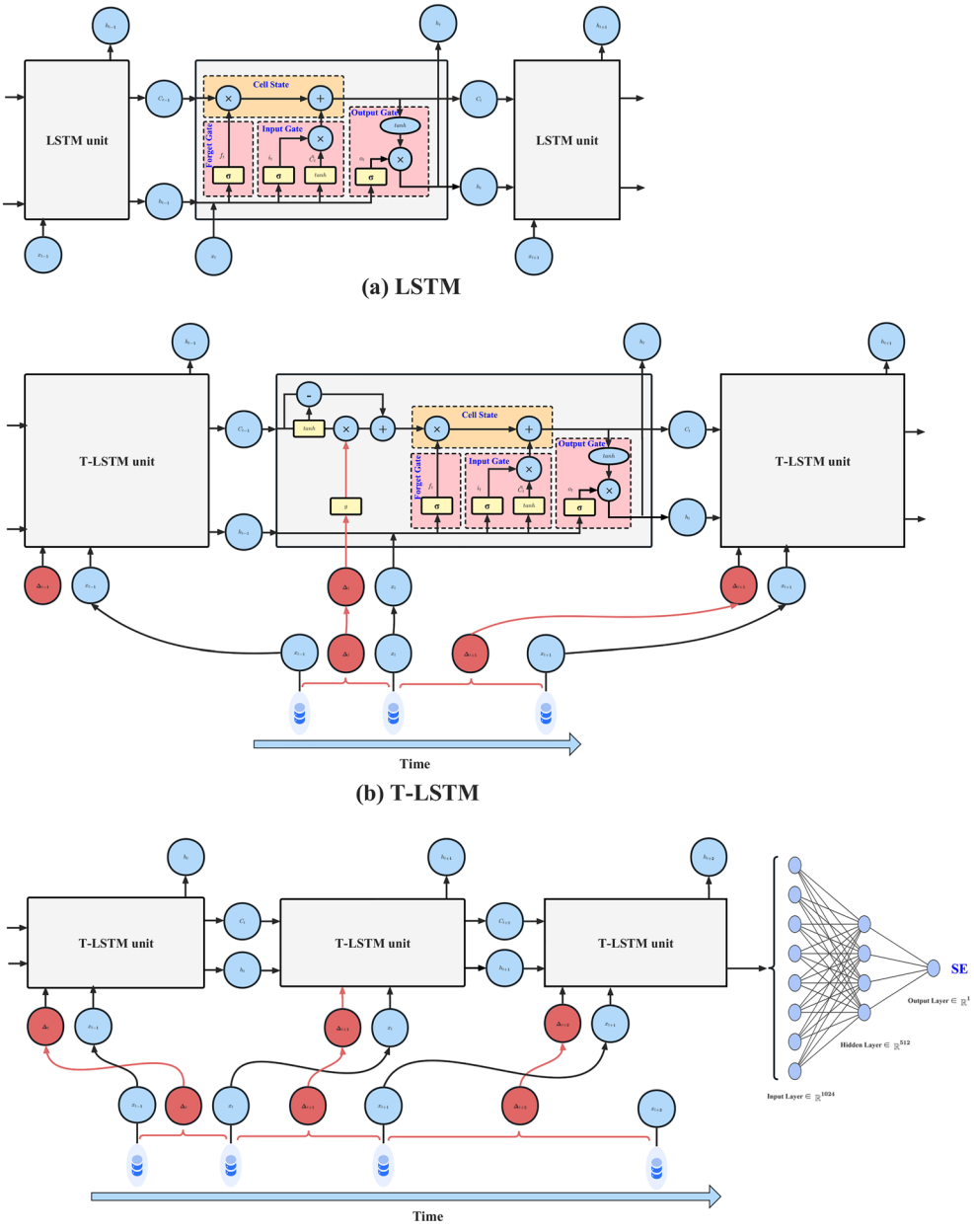

Figure 2. The structure of LSTM, T-LSTM and T-LSTM in myopia prediction, where x denotes the temporal input data, C is the cell state representing the long-term memory, h is the hidden state representing the short-term memory, Δ_t is the time interval between records x_t and x_{t-1}, σ is the sigmoid activation function, and *tanh* is the tanh activation function.

$$C^*_{t-1} = C^T_{t-1} + \hat{C}^S_{t-1}. \tag{11}$$

Application of T-LSTM in myopia prediction. The input of each cell of T-LSTM is the current record x_t and the time interval Δ_t between x_{t-1} and x_t. The output is the current state h_t. In the myopia prediction model proposed in this paper, the input of each cell is changed to the current record x_t and the time interval Δ_{t+1} between x_t and x_{t+1}. There are two kinds of inputs, namely records and time intervals. The record of an individual is an $n \times 16$ matrix containing n checks, and in each check there are 16 features (after the one-hot encoding, the number of features related to gender and correction method becomes 4). Correspondingly, the time intervals of this individual is a vector containing n time interval values. The last time interval value is the same to the prediction duration. The output is the next state h_{t+1}. The final prediction is the output of the last step which is passed through the fully connected neural network. The structure of the model is shown in Fig. 2c.

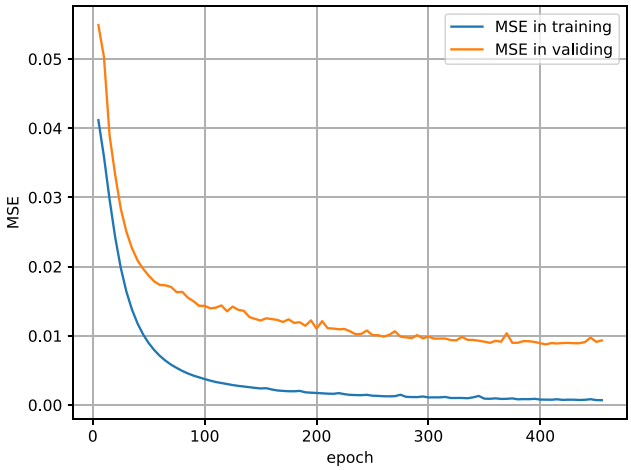

Figure 3. The change of MSE in the model. An epoch means training the neural network with all the training data for one cycle.

When performing myopia prediction, the values of visual acuity at any future moment can be predicted by changing the value of the last time interval. The training parameters of the model are as follows: Learning Rate = 0.0001, Batch Size = 256, Optimizer is Adam Optimizer, Epochs = 500, RNN Layers = 1, T-LSTM Hidden Size = 1024, and Early Stopping Patience = 10.

Metrics. The model's cost function is the mean square error (MSE) of SE, often referred to as the loss. The MSE lies in the range $[0, +\infty)$, as

$$MSE = \frac{1}{m}\sum_{i=1}^{m}(y_i - \hat{y}_i)^2, \tag{12}$$

where y_i is the actual value, $\hat{y}_i$ is the predicted value, and m is the number of samples. Equation (12) is a smooth, continuous and everywhere derivable function, and thus being convenient for the gradient descent algorithm. The prediction performance of the model is evaluated by the mean absolute error (MAE), which is the average of the absolute deviations, as

$$MAE = \frac{1}{m}\sum_{i=1}^{m}|(y_i - \hat{y}_i)|. \tag{13}$$

It takes values in the range of $[0, +\infty)$. A smaller MAE indicates a better model.

Ethics declarations. The experimental protocol was established, according to the ethical guidelines of the Helsinki Declaration and was approved by the Human Ethics Committee of University of Electronic Science and Technology of China (No. 106142022101324706). Written informed consent was obtained from individual or guardian participants.

Results

After 405 training iterations, the model converges with the loss (i.e., MSE) of the training process displayed in Figure 3. The MAE of future SE is 0.103 ± 0.140 (D) on the testing set. The stratified MAE is shown in Table 4. When sequence lengths are 1, 2, 3 and 4, the corresponding MAE ranges from 0.115 (D) to 0.187 (D) for 2 to 10 quarters, 0.082 (D) to 0.109 (D) for 2 to 6 quarters, 0.071 (D) to 0.079 (D) for 2 to 4 quarters and 0.040 (D) for 2 quarters, respectively. When the levels of myopia are no myopia, low myopia, moderate myopia and high myopia, the corresponding means and standard deviations of MAE are 0.116 ± 0.127 (D), 0.100 ± 0.136 (D), 0.094 ± 0.147 (D) and 0.153 ± 0.237 (D), respectively. When the age groups range from 6 to 8, 9 to 11, 12 to 14, 15 to 17 and 18 to 20, the corresponding means and standard deviations of MAE are 0.121 ± 0.156 (D), 0.099 ± 0.132 (D), 0.091 ± 0.128 (D), 0.088 ± 0.134 (D) and 0.056 ± 0.074 (D), respectively. Four case examples are shown in Fig. 4. The prediction curves well capture the trend of the SE changes while there are some unstable fluctuations that may be resulted from sparse records. Overall speaking, the longer the sequence length and the shorter the prediction duration, the smaller the prediction error. The MAE of SE within 0.75 (D) is considered to be a clinically acceptable prediction[13]. Based on the accuracy and robustness of the model, as well as the variance of the prediction performance, the model provides a clinically valuable prediction of children's and adolescents' vision in the short and medium term.

The result of the T-LSTM, standard LSTM, Random Forest (RF), and Linear Regression (LR) is shown as Table 5. Since LSTM, RF and LR do not specifically deal with time intervals, the time intervals are treated as

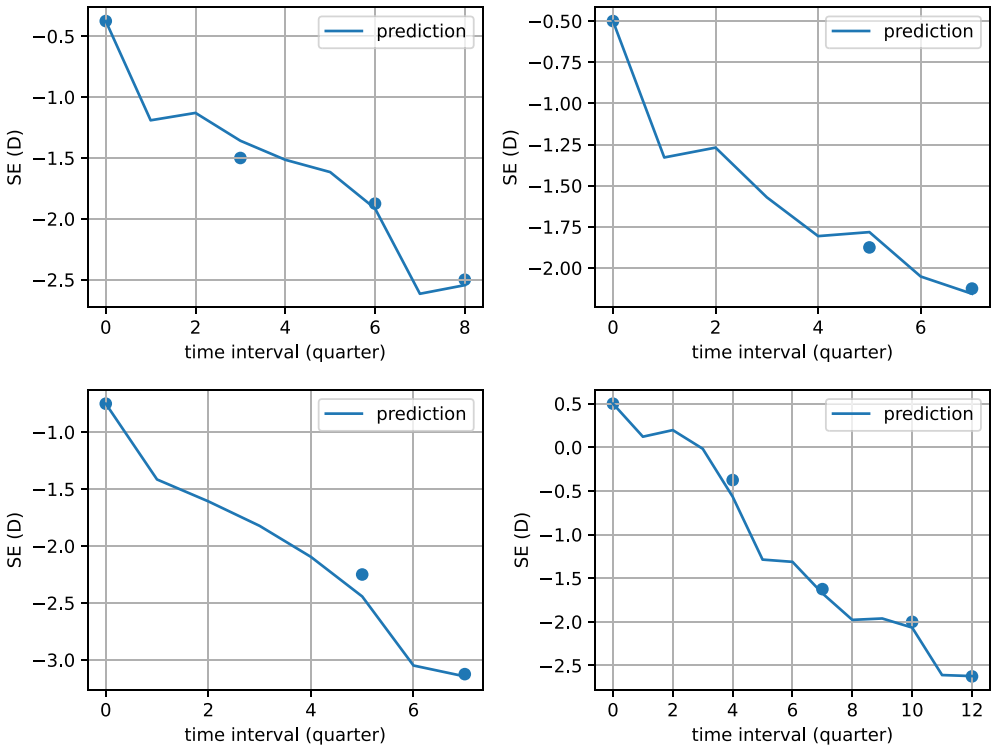

Figure 4. Four case examples of prediction using T-LSTM. In each example, the curve except the starting point means the predicted value, and the data points denote the true values.

Prediction duration[a]	The MAE of SE for different sequence lengths (mean ± standard deviation (sample size))[b]				Summary
	1	2	3	4	
1	*0.231 ± 0.195 (8)	*0.047 ± 0.064 (6)	*0.045 ± 0.046 (4)		*0.128 ± 0.162 (18)
2	0.115 ± 0.160 (4706)	0.082 ± 0.115 (6450)	0.071 ± 0.080 (3656)	0.040 ± 0.050 (432)	0.088 ± 0.124 (15244)
3	0.109 ± 0.145 (9269)	0.093 ± 0.142 (5239)	0.073 ± 0.089 (516)	*0.041 ± 0.000 (1)	0.102 ± 0.142 (15025)
4	0.118 ± 0.154 (4106)	0.088 ± 0.132 (3340)	0.079 ± 0.110 (494)		0.103 ± 0.143 (7940)
5	0.112 ± 0.136 (4339)	0.086 ± 0.130 (694)			0.109 ± 0.136 (5033)
6	0.130 ± 0.151 (3669)	0.109 ± 0.161 (505)	*0.040 ± 0.000 (1)		0.127 ± 0.152 (4175)
7	0.185 ± 0.197 (330)	*0.059 ± 0.000 (1)			0.184 ± 0.197 (331)
8	0.150 ± 0.153 (172)				0.150 ± 0.153 (172)
9	0.185 ± 0.187 (563)				0.185 ± 0.187 (563)
10	0.187 ± 0.168 (542)				0.187 ± 0.168 (542)
Summary	0.119 ± 0.151 (27704)	0.088 ± 0.130 (16235)	0.072 ± 0.085 (4671)	0.040 ± 0.050 (433)	0.103 ± 0.140 (49043)

Table 4. The MAE of SE in the testing set for T-LSTM. [a]A value i means the duration ranges from $i-1$ quarters to n quarters. [b]*Represents that the sample size is too small (< 100) to be a solid reference.

Model	The MAE of SE for different sequence lengths (mean ± standard deviation)				Summary
	1	2	3	4	
T-LSTM	0.119 ± 0.151	0.088 ± 0.130	0.072 ± 0.085	0.040 ± 0.050	0.103 ± 0.140
LSTM	0.172 ± 0.193	0.084 ± 0.138	0.076 ± 0.101	0.051 ± 0.078	0.133 ± 0.175
RF	0.156 ± 0.176	0.111 ± 0.141	0.099 ± 0.113	0.106 ± 0.106	0.135 ± 0.161
LR	0.325 ± 0.302	0.250 ± 0.230	0.212 ± 0.195	0.226 ± 0.180	0.289 ± 0.273

Table 5. Comparison of the MAEs of different models.

one additional feature added to the input records, and thus the input record of an individual in those models is an $n \times 17$ matrix. Because RF and LR can only handle fixed-length sequences, separated models were trained for different length sequences. As shown in Table 5, the overall MAE of T-LSTM is much better than the other three models. The reason why T-LSTM and LSTM outperform RF and LR lies in the fact that the former two models have the ability to capture long-term dependencies in data, and the reason why T-LSTM outperforms LSTM is that the former model can better capture temporal tendency by separately process temporal features.

Conclusions

As the symptoms of myopia are not typical, they are often ignored by parents in the early stages of development. However, if low myopia is not controlled, it can lead to high myopia and very serious blinding ocular complications, such as posterior scleral and macular degeneration, as well as a substantially higher chance of developing cataracts and glaucoma[30,31]. The earlier the onset of myopia, the more likely the eye axial length will elongate, the faster myopia will progress, and the higher the final diopter[32]. This paper can quantitatively predict the children's and adolescents' SE within two and a half years, and help to identify the progression of myopia earlier so that targeted interventions and corrective measures can be taken. This is of great significance for the prevention and control of myopia.

As the development of myopia is affected by a number of complex factors, such as heredity, environment, and behaviors[33,34], to achieve accurate myopia predictions is challenging. Deep learning is able to infer new features from the limited sets of features contained in the training set, while avoiding complex feature engineering. This paper applied T-LSTM to captured the temporal features in irregularly sampled time series, which is more in line with the characteristics of real data and thus has higher applicability.

Discussion

To the best of our knowledge, only a very small number of studies include quantitative predictions of future visual acuity. Among them, Lin et al.[13] achieved quantitative prediction of future SE in a study of nearly 130,000 people in Guangdong, China, 2018, where the MAE for 1 to 8-year SE prediction ranges from 0.253 to 0.799. This paper achieves higher prediction accuracy on a smaller dataset. In usual vision records, the uneven distribution of time intervals between historical records and the variable lengths of records make the utilization of temporal information very difficult for traditional methods. The proposed T-LSTM model is capable to handle data of indefinite sequence lengths, and can well capture temporal tendency by separately processing temporal features, even if the time intervals are irregular. This study can indicate the trend of refraction and visual acuity in the next two and a half years. The results are interesting not only for medical institutions to make statistics, but also for parents to see the level of vision loss more intuitively. In this way, it will guide guardians to take their children for timely myopia correction and early myopia prevention and control, which is more important and proactive than the post intervention by medical institutions and will contribute to the prevention and control of early myopia in children and adolescents.

The current study has some limitations. Firstly, This is a short follow-up period to analyze via T-LSTM. However, the visual test datasets with long time periods are rare and the current dataset is hard-won. In addition, even with the short period, the T-LSTM show remarkable advantage compared with other benchmark methods, and even the standard LSTM outperforms the linear regression. Secondly, the sample area is concentrated, and thus the representation is insufficient. Thirdly, the depth of longitudinal data still needs to be enhanced. Fourthly, myopia progression is related to many factors. For example, Juntae et al.[35] have found that retinal factors also contribute to myopic progression. However, our dataset only contains visual screening records and fundus images was not available in this study. Multimodal learning involving both fundus images and screening records may further improve the prediction accuracy.

Data availability

The data that support the findings of this study are available from Eye See Inc. but restrictions apply to the availability of these data, which were used under license for the current study, and so are not publicly available. Data are however available from the authors upon reasonable request and with permission of Eye See Inc.

Received: 18 October 2022; Accepted: 27 March 2023
Published online: 03 April 2023

References

1. Holden, B. A. *et al.* Global prevalence of myopia and high myopia and temporal trends from 2000 through 2050. *Ophthalmology* **123**, 1036–1042. https://doi.org/10.1016/j.ophtha.2016.01.006 (2016).
2. Organization, W. H. *World Report on Vision* (2019).
3. Sankaridurg, P. *et al.* Imi impact of myopia. *Investig. Ophthalmol. Vis. Sci.* **62**, 2. https://doi.org/10.1167/iovs.62.5.2 (2021).
4. Jong, M. *et al.* Consensus on myopia management for Asia. *Chin. J. Optom. Ophthalmol. Vis. Sci.* **24**, 161–169. https://doi.org/10.3760/cma.j.cn115909-20211125-00459 (2022).
5. French, A. N., Morgan, I. G., Mitchell, P. & Rose, K. A. Risk factors for incident myopia in Australian schoolchildren: The sydney adolescent vascular and eye study. *Ophthalmology* **120**, 2100–2108. https://doi.org/10.1016/j.ophtha.2013.02.035 (2013).
6. Fan, Q. *et al.* Childhood gene-environment interactions and age-dependent effects of genetic variants associated with refractive error and myopia: The cream consortium. *Sci. Rep.* **6**, 25853. https://doi.org/10.1038/srep25853 (2016).
7. Tedja, M. S. *et al.* Imi-myopia genetics report. *Investig. Ophthalmol. Vis. Sci.* **60**, M89–M105. https://doi.org/10.1167/iovs.18-25965 (2019).
8. Matsumura, S. *et al.* Annual myopia progression and subsequent 2-year myopia progression in Singaporean children. *Transl. Vis. Sci. Technol.* **9**, 12. https://doi.org/10.1167/tvst.9.13.12 (2020).
9. Han, X., Liu, C., Chen, Y. & He, M. Myopia prediction: A systematic review. *Eye* **36**, 921–929. https://doi.org/10.1038/s41433-021-01805-6 (2022).

10. Jones, L. A. *et al.* Parental history of myopia, sports and outdoor activities, and future myopia. *Investig. Ophthalmol. Vis. Sci.* **48**, 3524–3532. https://doi.org/10.1167/iovs.06-1118 (2007).
11. Chua, S. Y. L. *et al.* Age of onset of myopia predicts risk of high myopia in later childhood in myopic Singapore children. *Ophthalm. Physiol. Opt.* **36**, 388–394. https://doi.org/10.1111/opo.12305 (2016).
12. Mojarrad, N. G., Williams, C. & Guggenheim, J. A. A genetic risk score and number of myopic parents independently predict myopia. *Ophthalm. Physiol. Opt.* **38**, 492–502. https://doi.org/10.1111/opo.12579 (2018).
13. Lin, H. *et al.* Prediction of myopia development among chinese school-aged children using refraction data from electronic medical records: A retrospective, multicentre machine learning study. *PLoS Med.* **15**, e1002674. https://doi.org/10.1371/journal.pmed.1002674 (2018).
14. Ma, Y. *et al.* Cohort study with 4 year follow up of myopia and refractive parameters in primary schoolchildren in Baoshan district, shanghai. *Clin. Exp. Ophthalmol.* **46**, 861–872. https://doi.org/10.1111/ceo.13195 (2018).
15. Chen, Y. *et al.* Contribution of genome-wide significant single nucleotide polymorphisms in myopia prediction: Findings from a 10-year cohort of chinese twin children. *Ophthalmology* **126**, 1607–1614. https://doi.org/10.1016/j.ophtha.2019.06.026 (2019).
16. Yang, X. *et al.* Prediction of myopia in adolescents through machine learning methods. *Int. J. Environ. Res. Public Health* **17**, 463. https://doi.org/10.3390/ijerph17020463 (2020).
17. Huang, J. *et al.* Myopia contributing factors and myopia prediction based on vision examination data. *J. Univ. Electron. Sci. Technol. China* **50**, 256–260 (2021).
18. Vargas, R. & Lourdes, R. Previous and present applications. *Deep Learn. J. Awaren.* **2**, 11–20 (2018).
19. Siuly, S. & Zhang, Y. Medical big data: Neurological diseases diagnosis through medical data analysis. *Data Sci. Eng.* **1**, 54–64. https://doi.org/10.1007/s41019-016-0011-3 (2016).
20. Adam, G. *et al.* Machine learning approaches to drug response prediction: Challenges and recent progress. *NPJ Precis. Oncol.* **4**, 19. https://doi.org/10.1038/s41698-020-0122-1 (2020).
21. Jalali, A. *et al.* Deep learning for improved risk prediction in surgical outcomes. *Sci. Rep.* **10**, 9289. https://doi.org/10.1038/s41598-020-62971-3 (2020).
22. Sun, C., Hong, S., Song, M., Li, H. & Wang, Z. Predicting covid-19 disease progression and patient outcomes based on temporal deep learning. *BMC Med. Inform. Decis. Mak.* **21**, 45. https://doi.org/10.1186/s12911-020-01359-9 (2021).
23. Spadon, G. *et al.* Pay attention to evolution: Time series forecasting with deep graph-evolution learning. *IEEE Trans. Pattern Anal. Mach. Intell.* **44**, 5368–5384. https://doi.org/10.1109/TPAMI.2021.3076155 (2021).
24. Sree, K. P. N. V. S. *et al.* Optimized conversion of categorical and numerical features in machine learning models. In *2021 Fifth International Conference on I-SMAC (IoT in Social, Mobile, Analytics and Cloud) (I-SMAC)* 294–299 (2021). https://doi.org/10.1109/I-SMAC52330.2021.9640967.
25. Sharma, P. & Singh, J. Machine learning based effort estimation using standardization. In *2018 International Conference on Computing, Power and Communication Technologies (GUCON)* 716–720 (2018). https://doi.org/10.1109/GUCON.2018.8674908.
26. Pascanu, R., Mikolov, T. & Bengio, Y. On the difficulty of training recurrent neural networks. In *Proceedings of the 30th International Conference on Machine Learning*, vol. 28 1310–1318 (2013).
27. Zaremba, W., Sutskever, I. & Vinyals, O. Recurrent neural network regularization. arXiv:1409.2329 (2014).
28. Hochreiter, S. & Schmidhuber, J. Long short-term memory. *Neural Comput.* **9**, 1735–1780. https://doi.org/10.1162/neco.1997.9.8.1735 (1997).
29. Baytas, I. M. *et al.* Patient subtyping via time-aware lstm networks. In *Proceedings of the 23rd ACM SIGKDD International Conference on Knowledge Discovery and Data Mining* 65–74 (2017). https://doi.org/10.1145/3097983.3097997.
30. Saw, S.-M., Gazzard, G., Shih-Yen, E. C. & Chua, W.-H. Myopia and associated pathological complications. *Ophthalm. Physiol. Opt.* **25**, 381–391. https://doi.org/10.1111/j.1475-1313.2005.00298.x (2005).
31. Neelam, K., Cheung, C. M. G., Ohno-Matsui, K., Lai, T. Y. Y. & Wong, T. Y. Choroidal neovascularization in pathological myopia. *Prog. Retin. Eye Res.* **31**, 495–525. https://doi.org/10.1016/j.preteyeres.2012.04.001 (2012).
32. Hu, Y. *et al.* Association of age at myopia onset with risk of high myopia in adulthood in a 12-year follow-up of a Chinese cohort. *JAMA Ophthalmol.* **138**, 1129–1134. https://doi.org/10.1001/jamaophthalmol.2020.3451 (2020).
33. Guo, L. *et al.* Prevalence and associated factors of myopia among primary and middle school-aged students: A school-based study in guangzhou. *Eye* **30**, 796–804. https://doi.org/10.1038/eye.2016.39 (2016).
34. Choi, K. Y. *et al.* Childhood exposure to constricted living space: A possible environmental threat for myopia development. *Ophthalm. Physiol. Opt.* **37**, 568–575. https://doi.org/10.1111/opo.12397 (2017).
35. Kim, J. *et al.* Machine learning predicting myopic regression after corneal refractive surgery using preoperative data and fundus photography. *Graefes Arch. Clin. Exp. Ophthalmol.* **260**, 3701–3710. https://doi.org/10.1007/s00417-022-05738-y (2022).

Author contributions

W.M., R.L., N.Z. and T.Z. Conceived and designed the project. W.M. and R.L. collected the data. J.H. Performed the experiment. J.H., W.M. and T.Z. analyzed the data. J.H., W.M. and T.Z. wrote the manuscript. R.L. and N.Z. edited the manuscript.

Funding

The National Natural Science Foundation of China under Grant No. 11975071. Sichuan Science and Technology Program, China, under Grant No. 2022YFS0368.

Competing interests

The authors declare no competing interests.

Additional information

Correspondence and requests for materials should be addressed to W.M. or T.Z.

Reprints and permissions information is available at www.nature.com/reprints.

Publisher's note Springer Nature remains neutral with regard to jurisdictional claims in published maps and institutional affiliations.